

Radial-searching contour extraction method based on a modified active contour model for mammographic masses

Toshiaki Nakagawa · Takeshi Hara · Hiroshi Fujita ·
Katsuei Horita · Takuji Iwase · Tokiko Endo

Received: 8 January 2008 / Revised: 6 April 2008 / Accepted: 7 April 2008 / Published online: 8 May 2008
© Japanese Society of Radiological Technology and Japan Society of Medical Physics 2008

Abstract In this study, we developed an automatic extraction scheme for the precise recognition of the contours of masses on digital mammograms in order to improve a computer-aided diagnosis (CAD) system. We propose a radial-searching contour extraction method based on a modified active contour model (ACM). In this technique, after determining the central point of a mass by searching for the direction of the density gradient, we arranged an initial contour at the central point, and the movement of a control point was limited to directions radiating from the central point. Moreover, it became possible to increase the extraction accuracy by sorting out the pixel used for processing and using two images—an edge-intensity image and a degree-of-separation image defined based on the pixel-value histogram—for calculation of the image forces used for constraints on deformation of the ACM. We investigated the accuracy of the automated extraction method by using 53 masses with

several “difficult contours” on 53 digitized mammograms. The extraction results were compared quantitatively with the “correct segmentation” represented by an experienced physician’s sketches. The numbers of cases in which the extracted region corresponded to the correct region with overlap ratios of more than 81 and 61% were 30 and 45, respectively. The initial results obtained with this technique show that it will be useful for the segmentation of masses in CAD schemes.

Keywords Segmentation · Contour extraction · Active contour model · Mammographic mass · Computer-aided diagnosis

1 Introduction

Many techniques have been proposed for computer-aided diagnosis (CAD) in mammography, and several commercial (FDA-approved) CAD systems have been developed [1–3]. Most of them are systems for the detection of masses and clustered microcalcifications on mammograms. We are in the process of developing a CAD system for mammograms aimed at the automatic detection of masses [4, 5], architectural distortions [6], and clustered microcalcifications [7], characterization of their malignancy, and retrievals of similar cases [8].

In many CAD schemes for mammographic masses, features such as the shape, density, and contrast are computed from regions of mass candidates detected by a detection algorithm. Because radiologists closely observe the contours of masses when diagnosing the mammograms, the vital feature of a CAD system is its ability to evaluate the information conveyed by the contours. It is essential that the contours be extracted with a high degree

T. Nakagawa (✉) · T. Hara · H. Fujita
Department of Intelligent Image Information,
Division of Regeneration and Advanced Medical Sciences,
Graduate School of Medicine, Gifu University,
1-1 Yanagido, Gifu 501-1194, Japan
e-mail: nakagawa@fjt.info.gifu-u.ac.jp

K. Horita
Department of Radiology, Aichi Cancer Center Hospital,
1-1 Kanokoden, Chikusa-ku, Nagoya 464-8681, Japan

T. Iwase
Department of Breast Surgery, Cancer Institute Hospital,
1-37-1 Kamiikebukuro, Toshima-ku, Tokyo 170-8455, Japan

T. Endo
Department of Radiology, National Hospital Organization
Nagoya Medical Center, 4-1-1 Sannomaru, Naka-ku,
Nagoya 460-0001, Japan

of accuracy because the results obtained from the contour extraction in CAD schemes significantly affect a system's performance. To date, some techniques for the accurate contour extraction of masses have been reported [9–14]. Li et al. [9] used the Markov random-field model to detect masses. Petrick et al. [10] developed an adaptive contrast enhancement segmentation method to extract lesions. Kupinski and Giger [11] proposed a radial gradient index-based algorithm and a probabilistic algorithm that were seeded segmentation algorithms. However, because many masses often overlap with normal tissues, one of the issues that must be addressed is the more accurate and robust contour extraction in the case of masses that have partly indistinct contours. Sahiner et al. [14] applied an active contour model to the contour extraction of mammographic masses and quantitatively compared the results of the extraction with the manual segmentation performed by two radiologists. Consequently, the extents of area overlap in the results obtained by the two radiologists and the results obtained by a computer and the radiologists were 0.76 and 0.74, respectively. Despite the high extraction accuracy, fine irregularities in the contour were not extracted. Moreover, the extraction results were not very accurate and were unsuitable for shape recognition of the contour in our classification scheme, which analyzes the contours of benign and malignant masses by detecting the subtle sawtooth region of the mass contour. Timp et al. [15] proposed a dynamic programming-based segmentation method in which they used a polar-coordinate-converted image. However, the method did not solve the problem of locating the salient image contour but relied on another tissue near the desired contour. Moreover, it was necessary to determine manually the central point of a mass for precise contour extraction.

The contour extraction of a mass is always difficult because of the characteristics of the X-ray images. These characteristics are affected mainly by the fact that the background area in which a mass exists has a density slope, and that normal tissues such as the mammary glands and blood vessels can overlap the mass. Because of these less-than-ideal backgrounds, it is difficult to obtain the correct contour by using only a simple threshold method or region-growing method. In addition, it is necessary to include a technique that can distinguish normal tissues around the mass from the abnormal tissues in order to prevent the former from being extracted. Furthermore, because radiologists estimate unclear regions based on their anatomic knowledge or on the form of the contour that is apparent, extraction processing by a computer is also required for a technique that can perform the same estimate as do radiologists.

An active contour model (ACM) that Kass et al. [16] have proposed is a technique for contour extraction based

on the principle of minimization of the energy defined on a closed curve comprising control points. The ACM is useful in extracting the contour of an object at a high contrast against a background and for distinguishing smooth forms. However, its applicability is limited because it is unstable for detecting contours corresponding to mammographic masses that have relatively low contrast. Moreover, it is necessary to devise an automatic technique for setting the parameters as well as an initial contour at a position sufficiently close to the target because of the variations in the position, form, and size of a mass. This primary condition significantly influences the final result. In the case of variations in a mass, it is not easy to recognize the size, form, and position of the target beforehand, and in such cases, even if it is not desirable, the initial contour must be set up manually.

Our purpose in this study was to develop a contour extraction process based on our modified ACM (radial-searching contour extraction method) for recognizing the unclear contour of a mass. The details of the proposed technique are described as follows, and its validity is examined based on an experiment applied to mammographic masses.

2 Materials and methods

2.1 Overview of automated contour extraction method

Methods for evaluating unclear regions, for example, a simple threshold method or region-growing method, cannot be optimized because an underestimation of the region or region overflow often occurs. The ACM is one of the methods for extracting the object contour and an energy-minimizing spline, which consists of multiple control points, conducted by external and image forces that pull the spline curve toward the features of the object's contour in the image. An initial contour is first placed by the user manually or in some automatic way, and then the ACM deforms itself into conformity with the nearest salient contour by using an energy-minimization procedure.

When applying the conventional ACM method to a region where the contrast is low and the contour is ambiguous, it is often difficult to shift the control point to an ideal position. Moreover, it is necessary to devise an automatic technique for setting conditions such as an initial contour because of variations in the position, form, and size of a target. In order to tackle these issues, after the determination of the central point of a mass, we arranged an initial contour at the central point, and the movement of a control point was limited to directions radiating from the central point (Fig. 1). The central point of a mass was defined as a convergence point of the edge direction, which

was defined as the density gradient from each point on the mass contour, because the pixel values of the mass tend to increase toward the center. This process can prevent the control points from converging at positions of high intensity other than the mass; this is because the effect of an unclear contour can be determined based on the relationship between the position of the central point and a contour with relatively high contrast. The central point, in an ideal situation, is inside a contour and is located at a position equidistant from each point in the contour.

Moreover, it is possible to increase the extraction accuracy by choosing the pixel used for processing and using two images—an edge-intensity image and a degree-of-separation image defined based on the density histogram—for calculating the image forces of an ACM. Limiting the search range of the control points to a line segment made it possible to determine the unclear contour

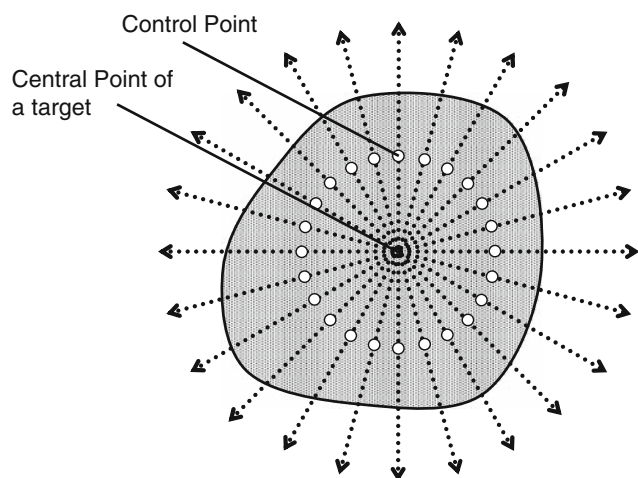


Fig. 1 Movement direction of the control points for searching for the contour

because it became possible to locate a control point even in the region where the edge intensity was low compared with that of the circumference. Next, the control point was moved radially from the center, and a set of control points that generate a minimum amount of energy was determined to be the contour of a mass.

An example in which this technique is applied to mass images on mammograms is given below, and the details of the technique are described in this section.

2.2 Determining the central point of a mass

As shown in Fig. 2a, in a mammogram, the mass appears whiter (higher density) than the surrounding tissue. Processing based on the threshold method determines the rough region of the mass, as shown in Fig. 2b, as the primary region detected by the detection algorithm for a mass in our CAD system [4]. The central point of the mass was determined by use of the primary region extracted by the detection technique of the CAD system. The control points were arranged with respect to the central point, and this arrangement was considered to be the initial contour. The central point of the mass is located near a convergence point of the edge direction defined as the density gradient from each point on the mass contour, because the pixel values of the mass tend to become high toward the center. Therefore, the position of the central point was determined by searching for the direction of the edge in the mass region.

The processing images are shown in Fig. 3. Erosion and dilation of the morphologic operation were performed on the original image [17, 18], i.e., in Fig. 3a, during the preprocessing for erasing the edge intensity of a calcification that made the accurate determination of the central point impossible when the calcification existed in the

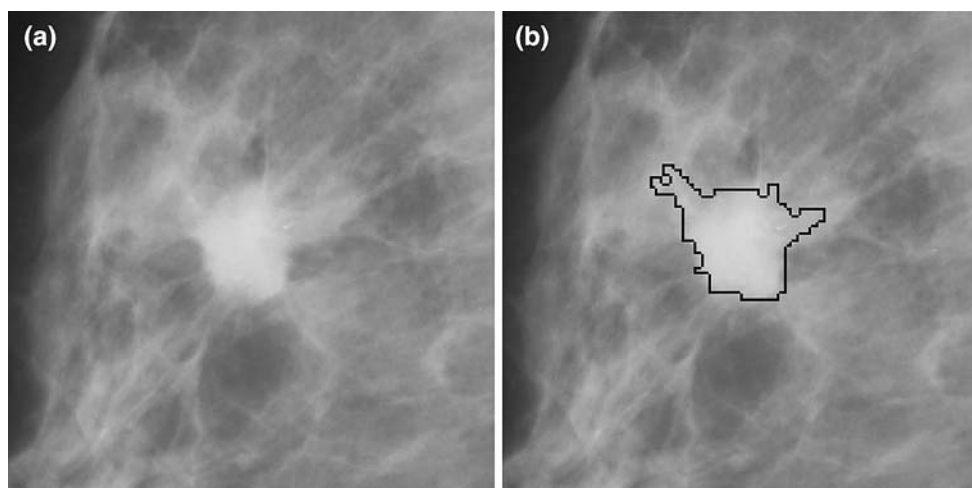


Fig. 2 Example of a mass on a mammogram. **a** Original image; and **b** a contour of primary detection region extracted by our CAD system

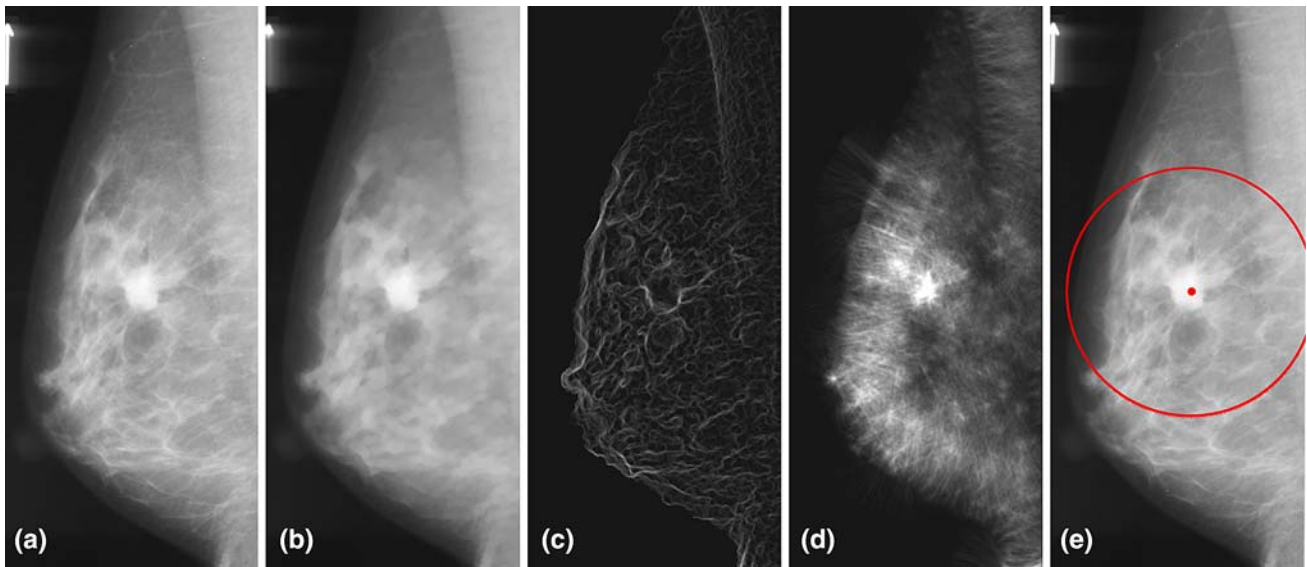


Fig. 3 Determination process for the central point of a mass. **a** Original image; **b** morphologic-processed image; **c** edge image; **d** edge-direction image; and **e** central point and area to be analyzed (*circle*)

mass region. A disc with a radius of 1 mm was used as a “structure element” used in the morphologic operation for erasing the calcification, taking into account its size. The edge image was developed from the pre-processed image by use of a Sobel filter [19]. The edge intensity near the skin line was higher than the contour edge intensity of the mass in the edge image, and the former might have a detrimental effect on the subsequent processing. Pixels whose value did not exceed 30% of the maximal value in the mass region were not used for the processing, because we wanted to exclude the region near the skin line from the processing. This threshold value defined as the percentage of the pixel value was determined by trial and error, such that the circumferential region of a mass was included and the low-density regions near the skin line were excluded from the analysis area. Although, ideally, the threshold value should be determined automatically for every image, a value was tentatively assigned for this study.

Next, the line segment was lengthened in the direction of the density gradient from each pixel of the edge image, and all of the line segments were added to form an image called the edge-direction image. The length of the line segment was set at 20 mm because the radius of the target mass was 20 mm or less; the width as 1 pixel; and the pixel value was set in proportion to the edge intensity. The point that had the maximum pixel value in this edge-direction image was determined as the central point of the mass. Figure 3e shows the central point that was determined (the dot in the figure) and the target area to be analyzed in the next step (inside the circle in the figure).

2.3 Pixel profiling by sorting-out of pixels

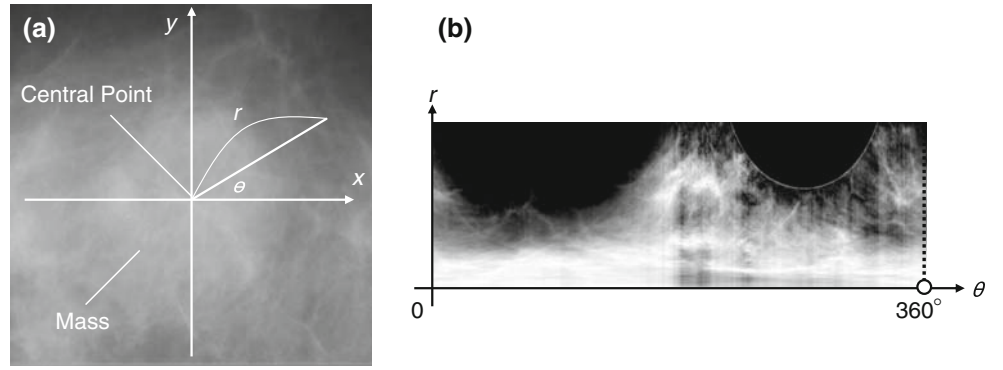
A line segment with a width of 1 pixel was lengthened radially from the central point of the mass, and the pixels on the line segment were profiled as

$$P_{\theta,r} = f_{c_x+r\cos\theta, c_y+r\sin\theta} \quad (0 \leq \theta < 360, \quad 0 \leq r < l), \quad (1)$$

where P represents the radial-profile image; f , the original image; (c_x, c_y) , the central point; r , the distance from the central point; θ , the direction of the line segment for the profiling; and l , the length of the line segment. This processing was performed in each direction from 0° to 360° for drawing the radial-profile image, as shown in Fig. 4. The contour extraction was performed by use of this radial-profile image. The conversion to polar coordinates was performed to simplify the processing, even though the extraction could be performed in rectangular coordinates. The length of the line segment was set to 40 mm because the size of the mass was comparable to a circle with a maximum radius of 20 mm, and 20 mm outside this hypothetical circle might be included as the background in an area to be analyzed. The interval angle of each line segment was set to 0.86° (418 divisions) to narrow the distance between the control points arranged at the contour of the target mass.

During pixel profiling, the edge of the contour was differentiated from the normal tissue as follows: as the position changes from the central point to the circumference, there is a tendency for the mass to have a low pixel value on the mammogram, and this value becomes high in the regions where normal tissues such as a mammary gland

Fig. 4 Transformation of coordinate system to form the radial-profile image. **a** Original image of a mass and **b** radial-profile image



or blood vessels are found. Therefore, the profile was executed only if a pixel value became low toward the outside from the central point, as follows:

$$P_{\theta,r} = \begin{cases} f_{c_x+r \cos \theta, c_y+r \sin \theta} (f_{c_x+r \cos \theta, c_y+r \sin \theta} \\ - f_{c_x+(r-1) \cos \theta, c_y+(r-1) \sin \theta} < 0) \\ f_{c_x+(r-1) \cos \theta, c_y+(r-1) \sin \theta} (f_{c_x+r \cos \theta, c_y+r \sin \theta} \\ - f_{c_x+(r-1) \cos \theta, c_y+(r-1) \sin \theta} < 0). \end{cases} \quad (2)$$

Moreover, if a pixel had a value less than 40% at the central point, the profiling was skipped because the low-density regions near a skin line or outside the breast region have to be eliminated from the target area.

The processing that distinguishes the masses from normal tissue is not necessarily effective in all cases, and an exact distinction cannot be expected. However, even if the normal tissue resembles a mass that is indistinct, its brightness barely increases from the center toward the circumference. The brightness may increase in cases where a mass overlaps the normal tissue. In order to distinguish the mass easily, we simply excluded the pixels in which the brightness increased from the center toward the circumference in the subjects of the analysis. It was predicted that this condition could exclude the edge of the normal tissue from the analysis area.

2.4 Images for calculating image force in ACM

A basic ACM model is a closed spline curve under the influence of the image forces that push the ACM toward image features like lines and edges [16]. The density slope of an image is generally used for calculating the image force. The density gradient, which is used in the Sobel filter, is determined by calculating the difference value not from the entire analysis area, but from the local area. Therefore, the control points of an ACM have the possibility to be attracted to singular points that are not a part of the mass contour. Moreover, indistinct contours complicate the process of contour extraction because the edge intensity of these contours has low values.

In order to accommodate this situation, we used discrimination analysis of the density distribution for the entire analysis area to guess the density of the contour. The density of the boundary between the mass region and the background was predicted by the pixel-value histogram of the pixels in each profile angle. The degree of separation calculated from the histogram indicates the suitability of a pixel value for dividing the histogram into two groups. This degree of separation is the distributed ratio λ given by the evaluation function [20] of the following formula:

$$\lambda \equiv \frac{\sigma_B^2}{\sigma_W^2}, \quad (3)$$

where σ_B and σ_W are inter- and intraclass variances, respectively.

$$\sigma_B^2 = \frac{1}{N} \left\{ n_1 (\mu_1 - \mu_0)^2 + n_2 (\mu_2 - \mu_0)^2 \right\} \quad (4)$$

$$\sigma_W^2 = \frac{1}{N} \left\{ \sum_{x=0}^T (x - \mu_1)^2 h(x) + \sum_{x=T+1}^M (x - \mu_2)^2 h(x) \right\}, \quad (5)$$

where $h(x)$ is the density (pixel value) histogram; M , the maximal pixel value; T , the threshold of the pixel value for the separation; and

$$N = \sum_{x=0}^M h(x) \quad (6)$$

$$n_1 = \sum_{x=0}^T h(x) \quad (7)$$

$$n_2 = \sum_{x=T+1}^M h(x) \quad (8)$$

$$\mu_0 = \frac{1}{N} \sum_{x=0}^M xh(x) \quad (9)$$

$$\mu_1 = \frac{1}{n_1} \sum_{x=0}^T xh(x) \quad (10)$$

$$\mu_2 = \frac{1}{n_2} \sum_{x=T+1}^M xh(x). \quad (11)$$

Examples of a radial-profile image, edge image, and degree-of-separation image are shown in Fig. 5. The edge image was formed by calculation of the density gradient from the central point to the outside at each pixel in each profile angle.

2.5 Energy-minimization procedure

Four hundred and eighteen control points were set to the position of the central point of each angle in the radial-profile image. The energy of an ACM was decided by the sum of the internal energy and image forces. The position of an ACM was represented by $v(s) = (x(s), y(s))$, $s = 1, \dots, N$. The energy function was defined as

$$E_{ACM} = \sum_{s=1}^N \{w_{int}E_{int}(s) + w_{image}E_{image}(s)\}, \quad (12)$$

where E_{int} represents the internal energy and E_{image} represents the image forces. The total energy, E_{ACM} , was defined as a combination of the two energy functions that was weighted by coefficients, w , N was 418, and w_{int} and w_{image} of the energy terms were set at 2 and 1, respectively.

The internal energy, E_{int} , served to impose a piecewise smoothness constraint and was calculated from the first-

and second-order derivatives with respect to the coordinates of the control points as follows:

$$E_{int}(s) = \{v(s+1) - v(s)\}^2 + \{v(s) - v(s-1)\}^2 + \{[\{v(s+1) - v(s)\} - \{v(s) - v(s-1)\}]\}^2. \quad (13)$$

The image forces were calculated from the edge image and degree-of-separation image. The weight coefficient for each energy term was determined by trial and error. The minimization procedure was an iterative technique; namely, each control point was moved by one pixel in the direction where the total energy becomes minimal among the pixels of the upper and lower sides of each control point. This processing was carried out until the energy converged.

2.6 Smoothing of edge image and degree-of-separation image by use of a Gaussian filter

The edge image and the degree-of-separation image were multiplied by the Gaussian filter, forming gradual slopes in order to prevent the control points from being interrupted at a position that did not possess the slope of the image force. The Gaussian filter was defined as

$$f(r) = e^{-r^2/2\sigma^2}. \quad (14)$$

The value of σ was set to the average of the distance from the central point to the point that was likely to have a contour. The assumed contour was determined by searching of the point with a maximum summation of the edge intensity and degree of separation for every profile angle, so that the control points were attracted to the area where the above two parameters were of high intensity. The value of σ gradually decreased as the convergence of the control points progressed. For example, when the energy-minimization procedure was repeated nine times, the value of σ was reduced to 9.0, and the variance was 1.0 in the final result of the contour extraction.

3 Results

The accuracy of the determination of the central point and that of the automated extraction method were evaluated on 53 masses with many “difficult contours” on 53 digitized mammograms. All of the mammograms were recorded by a screen/film system and digitized at 0.05-mm spatial resolution, 12-bit density resolution, and a density range of 0.0–4.0. The process of determination of the central point employed images reduced to 1/100 (0.5 mm/pixel) of the original images. The processing performed subsequently employed the images reduced to 1/6 (0.3 mm/pixel) of their original sizes.

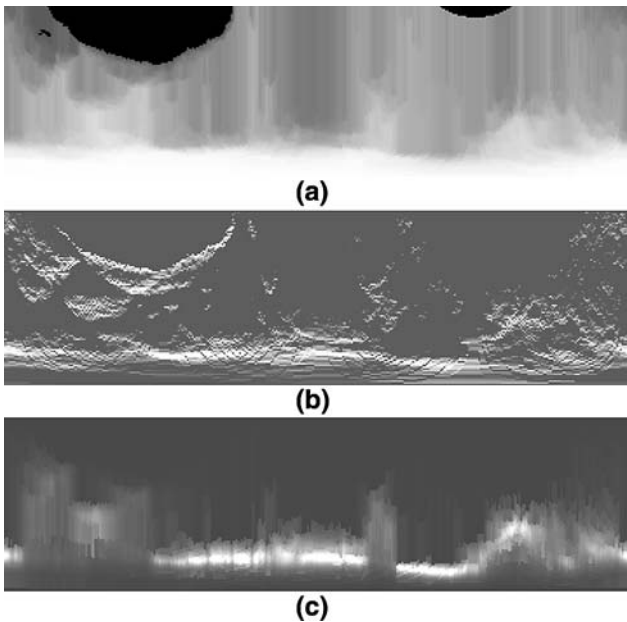


Fig. 5 Images for the active contour model. **a** Radial-profile image with sorting-out procedure; **b** edge image; and **c** degree-of-separation image. The *horizontal* and *vertical* axes correspond to the angle of the profile and the distance from the central point, respectively

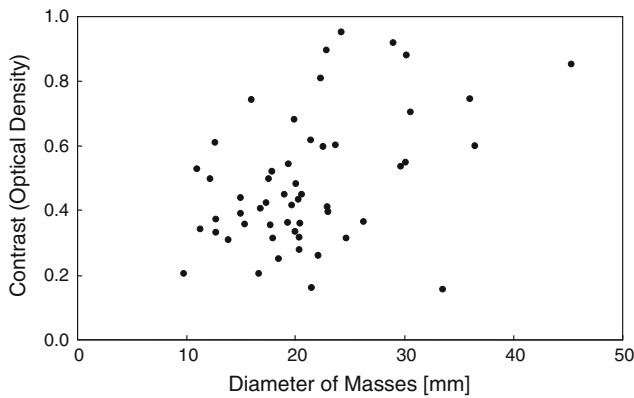


Fig. 6 Visibility distribution of the masses in a data set

Figure 6 shows the distribution plot of the contrast, which was defined as the difference in the optical density of a mass and its circumferential region, and the diameters of the masses in our database used for the simulation. The results of determining the central points of masses were evaluated subjectively by comparison with the sketches drawn by an experienced breast physician. The results of the automated extraction method were compared quantitatively with the “correct contours” drawn by a physician. The index for the estimation of the extraction accuracy was defined by the fraction of the area inside an extracted contour that overlapped with the region inside the “correct contour.” The overlap ratio was defined as follows:

$$\text{Overlap} = \frac{A_{\text{ext}} \cap A_{\text{cor}}}{A_{\text{cor}}}, \quad (15)$$

where A_{cor} and A_{ext} are the regions of the correct data and the extracted region, respectively. The error in the extraction was defined by the ratio of an extracted region to the region that did not overlap with the correct data. The error ratio was defined as follows:

$$\text{Error} = \frac{(A_{\text{ext}} \cup A_{\text{cor}}) - (A_{\text{ext}} \cap A_{\text{cor}})}{A_{\text{ext}} \cup A_{\text{cor}}}. \quad (16)$$

Figure 7 shows the difference in the pixel value and the degree of separation of a profile with and without the sorting-out procedure. In the case shown in the figure, the contour of the mass was located 20 pixels from the central point of the mass. The pixel value of the profile curve without the sorting-out procedure (indicated by crosses in the figure) gradually became low as the position deviated from the central point, and the pixel value rose from 30 pixels, which was a mammary-gland region. Furthermore, the pixel value rose again at 50 pixels after a decline, and decreased from near by 60 pixels. The edge intensity became comparatively high in the positions with an increase in the pixel value. In contrast, there was no density change in the profile curve with the sorting-out procedure (indicated by dots in the figure) because the pixel value

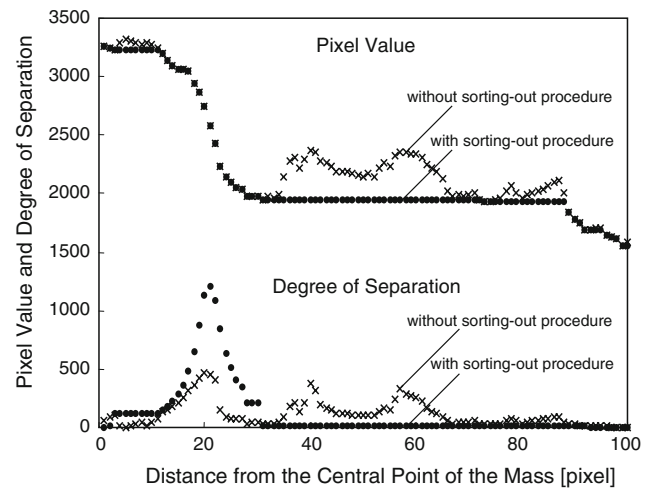


Fig. 7 Difference in the pixel value and degree of separation of a profile with and without the sorting-out procedure

variance in the mammary-gland region located from 30 to 70 pixels was planarized.

Moreover, the distribution curve of the degree of separation with the sorting-out procedure (indicated by dots in the figure) had only one high peak, which appeared near the position of the mass contour. Therefore it was easy to search the contour, even though there were three peaks in the distribution curve of the degree of separation without the sorting-out procedure (indicated by crosses).

Figure 8 shows the result obtained when this technique was applied to the mass of Fig. 2 and the sketch drawn by a physician. There was a small difference concerning the low-contrast region between the contour of the physician’s sketch and that of the primary detection result obtained with our CAD system, as indicated in Fig. 2b. However, the unclear contour that was found in the upper left portion of the mass was improved, and on the whole, the results were good.

In the determination of the central point of the masses, the central point could be determined correctly in 89% (41/46) of the cases examined, when the seven cases the cause of whose cause of failure was a mistake in the rough extraction step of our mass-detection algorithm were counted out. The correct answer for the central point was assumed to be the barycentric coordinate of a mass region, which had been determined subjectively. A small extent of displacement of the central point did not always have an adverse affect on the accuracy of the contour extraction because the ACM was sufficiently flexible for compensating for the resulting irregularities in the contour.

The automated extraction method was compared quantitatively with the correct segmentation represented by sketches made by a well-experienced physician. The results are shown in Fig. 9. The numbers of cases in which the extracted region corresponded to the correct region with

Fig. 8 An example of extraction result. **a** Automatically extracted contour of the image shown in Fig. 1; and **b** its sketch drawn by a physician

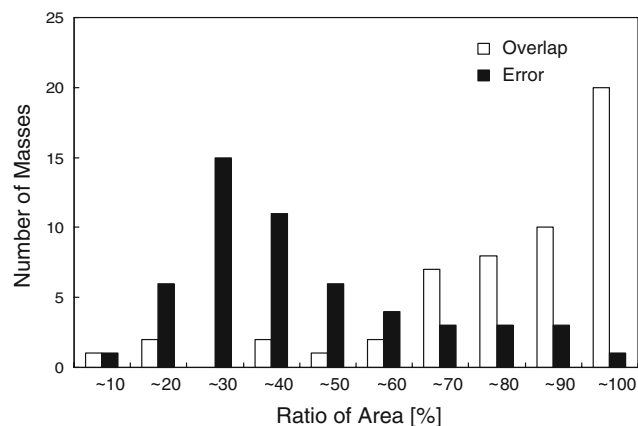
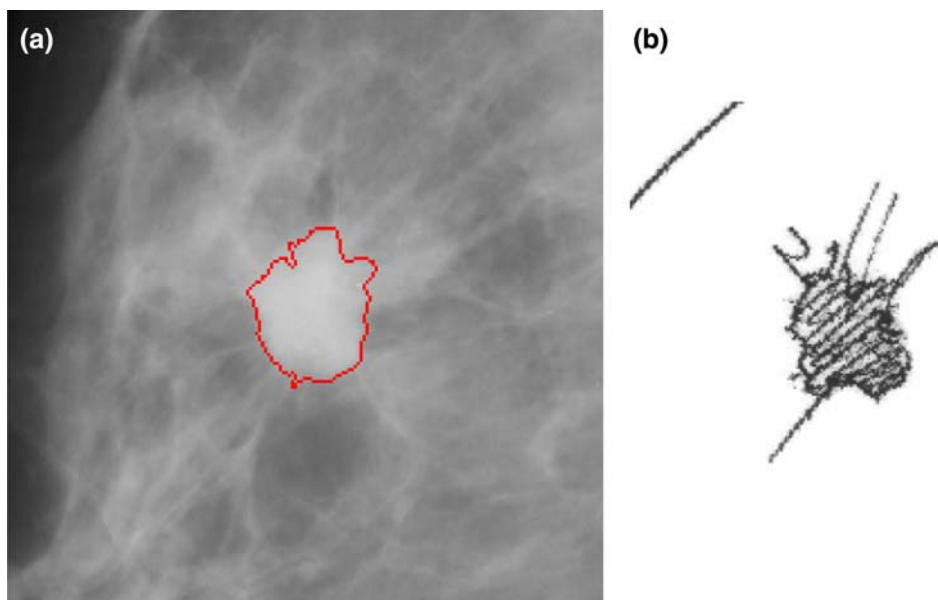


Fig. 9 Ratio distribution of area between the extracted results and the regions inside "correct contour"

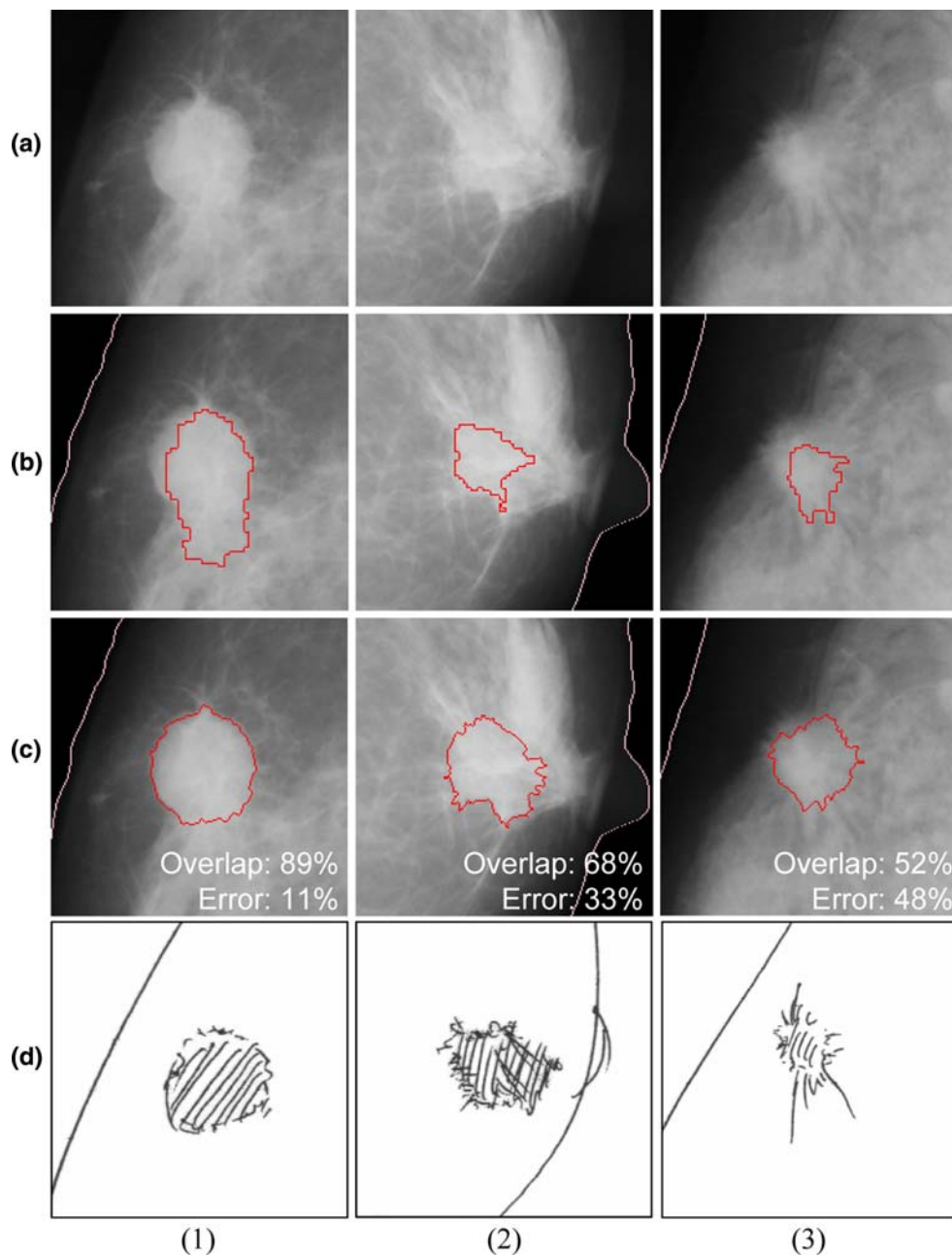
overlap ratios of more than 81 and 61% were 30 and 45, respectively. Many cases were observed wherein the extracted region corresponded to the correct region. Moreover, the regions extracted by the proposed technique were extremely precise as compared with the primary detection regions extracted by the adaptive threshold method in our CAD system; however, in some cases, the area did not correspond to the correct region. The contour extraction was difficult for some of the masses having indistinct contours in total or in part, and the error ratios were more than 60%. These were difficult even for a physician to observe and determine. The extracted region tended to be large when the size and contrast of the masses were small.

Figure 10 shows examples of the contour extraction results. The degrees of congruence and error were 89 and 11%, respectively, in case 1; 68 and 33% in case 2; 52 and 48% in case 3. The degree of congruence was high and the

error was small in cases where the contour of the mass was circular, as in case 1. The masses with a high contrast and clear contours were extracted with comparatively good accuracy, although an irregular mass similar to that in case 2 tended to have a low degree of congruence as compared with case 1. In some cases involving masses with several contours, the size of the mass was smaller than that expected, and the contrast was low, similar to that in case 3; the extraction results included the area external to the correct region, and the error area was large. When the masses were fairly visible with distinct contours, the results were good. The contour extraction results for masses that had a low contrast and an unclear region differed from those obtained by the physician, and when no clear contours were apparent, this difference was more marked. Moreover, there were few cases with adequate extraction in the region where the sketch was not drawn because the observation was difficult even for a physician. However, in many cases, when the mass contained some unclear regions, it was possible to form a valid contour in these regions by connecting the points that had a high probability of forming the correct contour. This probability was estimated based on the relationship between the position of the central point and the relatively distinct contour.

As a part of the CAD system, we have also been developing a scheme for the classification of breast masses on mammograms [21]. The classification system extracts various features such as density, contrast, shape type, and spiculation from the mass regions. The extracted contours of 52 masses (10 benign and 42 malignant) were fed into the benign/malignant classification system. The performance of the system with regard to different contours was evaluated, and the results are shown in Table 1. With use of the correct,

Fig. 10 Three segmentation examples: **a** Original images; **b** primary detection regions by the CAD system; and **c** segmentation results. **d** Physician's sketches for comparison



manually drawn contours, the benign/malignant classification accuracy was 85% (44/52). However, the classification accuracies obtained by use of the contours produced by the modified active contour model and our conventional segmentation method based on the adaptive thresholding method were 79% (41/52) and 65% (34/52), respectively.

4 Discussion

Our technique was applied to masses whose contour extraction was difficult when the simple threshold method was used. A precise contour extraction was obtained in

many cases in which the pixel values of the mass regions were partly equivalent to the background. This result showed that searching for the contour in the direction radiating from the central point of the mass and determining the contour based on the local density gradient and global density distribution could reduce the influence of the density gradient of the background around the mass. Moreover, using only the pixel whose value became low toward the outside from the central point could reduce the influence of the density or edge intensity, such as in the case of a mammary gland.

These advantageous effects could make the distinction between a mass contour and normal tissue easier, and thus

Table 1 Classification results using the contours extracted by the adaptive threshold method and radial-searching contour extraction method, and “correct contours” drawn by a physician

	Benign	Malignant	Total
Adaptive threshold method	20% (2/10)	76% (32/42)	65% (34/52)
Radial-searching contour extraction method	50% (5/10)	86% (36/42)	79% (41/52)
Correct contour	70% (7/10)	88% (37/42)	85% (44/52)

simplify the extraction process. The results show that the possibility that the extraction would be successful even at low-density gradients was increased by use of two images—the edge intensity and the degree of separation—for the image force of the ACM. Furthermore, this technique was effective in cases with partly unclear regions because of the following advantageous effect: the unclear contour’s position was presumed from the relationship between the central point of the mass and the distinct contour. However, if the central point was determined as the position in which the lengths from each point on the correct contour differed considerably, the extraction might not succeed. This is because it was difficult for the gradual density gradient of a Gaussian filter to attract the control points of the ACM to the position of the correct contour. Therefore, if the accuracy of the method for determining the central point is increased, it is to be expected that the level of accuracy of the contour extraction will also increase. Additionally, there is a limitation that this method cannot be applied to cases in which the shape of a mass is vastly different from a circle or an ellipse, because there will be several contours on the line segment lengthened radially from the central point of the mass in such cases.

In certain cases involving very small contours, the extraction was not possible because of the difficulty in the determination of the central point. One of the causes of the extraction failure also lay in the various radii of the masses listed in the database, although the assumed radius of the target mass was 10–20 mm in this study. The data used for this study were obtained at a cancer center, rather than from screening mammography. Although small masses should be targeted for detection, we believe that the CAD system can be used satisfactorily for the classification of large masses. One of the ACM’s parameters with respect to the size of masses was set as 10 mm in this study because there were many relatively large masses in the dataset. However, this parameter should be adjusted to a smaller value when this technique is applied to screening mammography or, more specifically, is optimized dynamically depending on the size of a target mass. This will be a subject for our future studies.

The parameters of the ACM segmentation model such as coefficients of the energy terms may have been overtrained because the data set was relatively small. Although public databases such as that of the University of South Florida contain many cases and serve many purposes, there are no detailed data on the contours of masses required for the shape recognition of the contour in our classification scheme, which analyzes the contour by detecting the subtle sawtooth region of the mass contour. Therefore, our local database was used for this study. However, it is necessary to evaluate the performance of this model in the future by using many precise data. Additionally, measuring the geometric matching distance such as the Hausdorff distance [14] would be better as an additional, more precise evaluation criterion. The performance of the extraction method was evaluated by the overlap and error ratio in this study; however, this criterion might not be reflected in the correspondence between the two regions in the details of the contour.

When the automatically extracted contours produced by the modified ACM were used, the benign/malignant classification system achieved an accuracy of 79% (41/52). This classification accuracy was higher than that (65% (34/52)) of our conventional segmentation method, which is based on the adaptive thresholding method. These results demonstrate the feasibility of using the modified active contour model for classifying benign and malignant masses on mammograms in a computer-aided diagnosis scheme.

5 Conclusion

We developed a contour extraction technique based on a modified ACM for masses on mammograms, and we evaluated its performance. Valid results were obtained from the experiments involving masses whose contours were difficult to extract. This technique will be useful for the segmentation of masses in CAD schemes.

Acknowledgments This study was supported in part by a Grant-in-Aid for Scientific Research from the Japan Society for the Promotion of Science, a Grant-in-Aid for Cancer Research from the Ministry of Health, Labour and Welfare, Japan, and a grant for the “Intellectual Cluster Creation Project” from the Ministry of Education, Culture, Sports, Science and Technology, Japan. We are grateful to reviewers for their helpful comments and suggestions, and the Editorial Assistant for providing detailed suggestions for improving this manuscript.

References

1. Hologic, Inc., R2 ImageChecker[®], <http://www.r2tech.com/>.
2. iCAD, Inc., SecondLook[®], <http://www.icadmed.com>.
3. Eastman Kodak Company. Kodak Mammography Computer-Aided Detection System, <http://www.Kodak.com>.

4. Matsubara T, Fujita H, Hara T, Kasai S, Otsuka O, Hatanaka Y, et al. New algorithm for mass detection in digital mammograms. Proceedings of CARS (Computer Assisted Radiology and Surgery) '98. 1998; International Congress Series 1165:219–23.
5. Hatanaka Y, Hara T, Fujita H, Kasai S, Endo T, Iwase T. Development of an automated method for detecting mammographic masses with a partial loss of region. *IEEE Trans Med Imag.* 2001;20:1209–14.
6. Matsubara T, Ichikawa T, Hara T, Fujita H, Kasai S, Endo T, et al. Automated detection methods for architectural distortions around skinline and within mammary gland on mammograms. Proceedings of CARS (Computer Assisted Radiology and Surgery) 2003. 2003; International Congress Series 1256:950–5.
7. Ibrahim N, Fujita H, Hara T, Endo T. Automated detection of clustered microcalcifications on mammograms: CAD system application to MIAS database. *Phys Med Biol.* 1997;42:2577–89.
8. Nakagawa T, Hara T, Fujita H, Iwase T, Endo T. Image retrieval scheme for mammographic masses by using a local pattern matching technique. Proceedings of CARS (Computer Assisted Radiology and Surgery) 2002. 2002;665–70.
9. Li HD, Kallergi M, Clarke LP, Jain VK, Clark RA. Markov random field for tumor detection in digital mammography. *IEEE Trans Med Imag.* 1995;14:565–76.
10. Petrick N, Chan HP, Wei D, Sahiner B, Helvie MA, Adler DD. Automated detection of breast masses on mammograms using adaptive contrast enhancement and texture classification. *Med Phys.* 1996;23:1685–96.
11. Kupinski MA, Giger ML. Automated seeded lesion segmentation on digital mammograms. *IEEE Trans Med Imag.* 1998;17:510–7.
12. Brake GM, Karssemeijer N. Segmentation of suspicious densities in digital mammograms. *Med Phys.* 2001;28:259–66.
13. Li H, Wang Y, Liu KJ, Lo SC, Freedman MT. Computerized radiographic mass detection—part I: lesion site selection by morphological enhancement and contextual segmentation. *IEEE Trans Med Imag.* 2001;20:289–301.
14. Sahiner B, Petrick N, Chan HP, Hadjiiski LM, Paramagul C, Helvie MA, et al. Computer-aided characterization of mammographic masses: accuracy of mass segmentation and its effects on characterization. *IEEE Trans Med Imag.* 2001;20:1275–84.
15. Timp S, Karssemeijer N. A new 2D segmentation method based on dynamic programming applied to computer aided detection in mammography. *Med Phys.* 2004;31:958–71.
16. Kass M, Witkin A, Terzopoulos D. Snakes: active contour models. *Int J Comput Vis.* 1987;1:321–31.
17. Serra J. Introduction to mathematical morphology. *Comput Vis Graphics Image Process.* 1986;35:283–305.
18. Sternberg SR. Grayscale morphology. *Comput Vis Graphics Image Process.* 1986;35:333–55.
19. Parker JR. Algorithms for image processing and computer vision. New York: Wiley Computer Publishing 1997.
20. Otsu N. A threshold selection method from gray-level histograms. *IEEE Trans Syst Man Cybern.* 1979;SMC-9:62–6.
21. Nakagawa T, Sakurai H, Hara T, Fujita H, Iwase T, Endo T, et al. Development of automatic classification system for mammographic masses: saw-tooth region detection method for recognition of mass contour shapes (Japanese). *Trans Jpn Soc Med Biol Eng.* 2005;43:437–46.